Numerical simulation of particle motion in a phase modulated surface acoustic wave microfluidic device

Numerical simulation of particle motion in a phase modulated surface acoustic wave microfluidic device

Gergely Simon
School of Engineering and Physical Sciences
Heriot-Watt University
Edinburgh, United Kingdom
g.s.simon@ieee.org

Marco A.B. Andrade
Institute of Physics
University of São Paulo
São Paulo, Brazil
marcobrizzotti@gmail.com

Mathis O. Riehle
Centre for Cell Engineering, Institute for Molecular, Cell and Systems Biology, CMVLS
University of Glasgow
Glasgow, United Kingdom
Mathis.Riehle@glasgow.ac.uk

Marc P.Y. Desmulliez
School of Engineering and Physical Sciences
Heriot-Watt University
Edinburgh, United Kingdom
m.desmulliez@hw.ac.uk

Anne L. Bernassau
School of Engineering and Physical Sciences
Heriot-Watt University
Edinburgh, United Kingdom
A.Bernassau@hw.ac.uk

***Abstract*—Contactless sorting of particles and cells in microfluidic devices is beneficial for various industrial and scientific applications. Among such techniques, acoustic sorting methods are favored for their reconfigurability and label-free processing capabilities. A phase modulated sorting method is proposed in this article as an alternative to time-of-flight sorters. The method has been analyzed theoretically and experimentally validated by considering the primary acoustic radiation and viscous drag forces. However, in real devices, acoustic streaming that arises from the damping of acoustic waves within the fluid cavity can adversely affect sorting. This paper presents therefore a numerical study of the influences that the primary radiation force and acoustic streaming can have on the phase modulated sorting method. The article highlights the existence of a critical particle size, above which acoustic streaming effects governing the behavior of small size particles are dominated by the primary radiation force. The model is extended for trajectory simulation in phase-modulated fields and validated with experimental data.**

Keywords—acoustic tweezing, acoustic radiation force, acoustic streaming, numerical simulation, phase modulation

I. Introduction

Separation of cells or particles from heterogeneous mixtures or suspensions is essential in many applications ranging from biomedical research, chemical analysis to industrial processing [1]. A wide range of microfluidic systems are available, covering low-cost, disposable passive sorters and more complex active techniques [2]. Acoustic methods combine the advantages of these systems by offering reconfigurable devices at moderate cost while maintaining cell viability and eliminating the need for labelling target entities [3]. Most acoustic techniques use static standing wave fields to achieve sorting based on the size-dependent velocities of particles. Our phase modulated method, in contrast, offers a dynamic control of the acoustic field, allowing particles and cell sorting in both bulk and continuous flow surface acoustic wave devices with less sensitivity of flow rate variations [4-6]. In this article, we use numerical simulations [7, 8] to investigate the influence of the acoustic radiation force and the acoustic streaming on the phased modulated sorting method.

II. Method

Particles or cells subjected to a standing acoustic wave experience an acoustic radiation force, F_{rad}, [9] given by

$$F_{\mathrm{rad}} = V_{\mathrm{p}} k E_{\mathrm{ac}} \Phi_{\mathrm{AC}} \sin(2kx), \tag{1}$$

where V_p is the volume of the particle, k is the wavenumber, E_{ac} is the acoustic energy density and Φ_{AC} the acoustic contrast factor, which depends on the density and compressibility of particle and fluid. Most particles and cells are directed towards the pressure nodes by the radiation force. The acoustic radiation force in a fluid medium is opposed by the drag force

$$F_{drag} = -c_{\mathrm{visc}} a \dot{x}, \tag{2}$$

where c_{visc} depends on the fluid viscosity and a is the particle radius. As the two forces scale differently with particle size, different movements can be observed that are based on particle size, enabling thereby particles separation [9].

Our method can be described by the aid of Fig. 1. A standing wave is generated in the microchannel by two opposing surface acoustic wave transducers. The positions of the pressure nodes are controlled by changing the relative phase between the transducers. Particles are initially trapped by the stationary standing wave at the bottom pressure node (Fig. 1c left). The linear phase modulation (Fig. 1a) of one transducer directly translates to the movement of the pressure nodes (Fig. 1b), dragging the particles laterally in the channel. However, due to the scaling of forces, the particles of various sizes arrive at locations on different sides of the pressure antinode when the phase shift ends (Fig. 1c middle). Afterwards the phase is kept constant, ensuring that the two particles relax to different nodes completing thus the sorting cycle (Fig. 1c right).

This method has already been validated against an analytical model in our previous studies [5, 6]. This paper focuses on a COMSOL validation method that uses a numerical model based on the work of Devendran *et al.* [8]. The model uses the thermoviscous acoustics, laminar flow and particle trajectories modules present in the software package. The thermoviscous acoustics module is used to simulate in the frequency domain the pressure and velocity fields within the

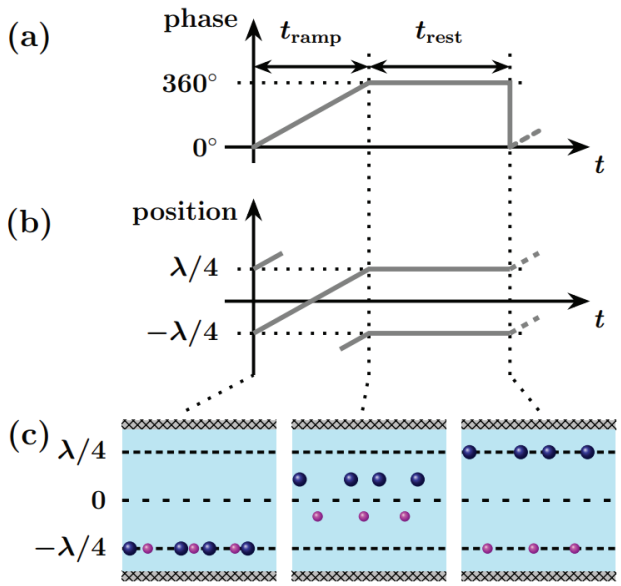

Fig. 1. Illustration of the phase modulated sorting method. (a) The phase pattern applied on one transducer (b) The resulting movement of the position of the pressure nodes (c) The particles are initially trapped at the bottom pressure node (left) and are dragged to be positioned on different sides of the pressure antinode after the ramping time (middle graph) and move towards different final positions during the resting period (right graph).

channel. These results are passed onto the laminar flow module to obtain the streaming velocity fields in a stationary study. Finally, the acoustics fields are used to calculate the radiation force, while the streaming fields result in the viscous drag force, which are coupled in a time domain particle tracing study to obtain particle trajectories.

Instead of a computationally extensive 3D model, we only simulated the rectangular cross-section of the microchannel and substituted the PDMS and the substrate with the appropriate boundary conditions (BC). For the two sides and the top of the channel, the PDMS is modelled as a normal impedance BC of characteristic impedance $Z = \rho_{\mathrm{PDMS}} c_{\mathrm{PDMS}}$, which is the product of density and bulk sound speed. The surface waves travelling in opposite directions on the lithium niobate substrate are applied as velocity BCs at the bottom of the microchannel. As the surface acoustic waves follow an elliptical motion, the x and y velocity components are 90° out of phase with respect to each other and the sign of the y component should agree with the travelling direction of the wave [8]. Two changes are necessary to these equations to be able to model our device and sorting method: the phase difference of the two transducers should be added, and, as the microchannel is not exactly an integer multiple of half the wavelength, an additional phase shift is required to have the adequate reference frame used in COMSOL. Therefore, the velocity boundary condition in the x and y directions have the following form:

$$v_x = \zeta d_0 \omega \left[\exp\left(-C_d(W/2-x)\right)\exp\left(-i\left(k_0(W/2-x)\right)\right) + \exp\left(-C_d(W/2+x)\right)\exp\left(i(k_0(W/2-x)+\varphi_0+\Delta\varphi)\right)\right], \quad (3)$$

$$v_y = -d_0 \omega \left[\exp\left(-C_d(W/2-x)\right)\exp\left(-i(k_0(W/2-x)-\pi/2)\right) - \exp\left(-C_d(W/2+x)\right)\exp\left(i(k_0(W/2-x)-\pi/2+\varphi_0+\Delta\varphi)\right)\right], \quad (4)$$

where ζ is the ratio of displacement amplitude in the x and y directions, d_0 is the y-displacement amplitude of the travelling wave, ω is the angular frequency, C_d is the attenuation coefficient, W is the width of the channel and k is the wavenumber. The phase values φ_0 and $\Delta\varphi$ correspond to the shift of the reference frame and the phase difference between transducers, respectively. A positive phase difference results in a rightwards movement of the pressure distribution. For the fluid domain a thermoviscous acoustics physics module was utilized with P2+P3 discretization (second order elements for pressure and third order elements for velocity) to be able to capture small variations in the pressure and velocity fields. The most important simulation parameters are listed in Table I, the thermoviscous-related values are the same as in [8]. The laminar flow physics used a stick wall boundary condition. To obtain the drag force, the built-in force feature inherent to COMSOL was used, which directly implements Eq. (2) using the streaming velocity fields from the laminar flow simulations, and an explicit equation for the acoustic force was given, as detailed in [7].

To obtain particle trajectories the simulation model had to be expanded to include the phase modulation scheme. As the continuous phase modulation cannot be included in the frequency domain study, we used a 10-step discretization of the ramping signal (Fig. 1a) as follows: the first step is taken at 18° phase difference, and increments of 36° are used up to 342°. For each case, a frequency domain study computes the acoustic pressure and acoustic velocity fields, which are used in the laminar flow module for simulation of the streaming velocity fields. 11 steps are present within the time domain simulation: the first 10 steps each correspond to one of the above described phase discretization during ramping; the last one corresponds to the resting phase, with zero phase.

In order to capture the thermoviscous effects while avoiding a high computational demand, a non-uniform mesh was applied. First, we computed the viscous boundary layer thickness $\delta_v = \sqrt{2\eta/\rho\omega} \approx 0.15$ µm, and used it with a scaling parameter N_{mesh} to define the mesh at the boundaries and in the bulk of the fluid. At the boundaries, the maximum element size was set for $N_{\mathrm{mesh}}\delta_v$, while in the bulk of the fluid, the minimum element size was $N_{\mathrm{mesh}}\delta_v$ and the maximum element size 2 µm. A mesh convergence analysis was carried out to determine the appropriate N_{mesh} value,

TABLE I. MOST RELEVANT PARAMETERS USED IN THE NUMERICAL SIMULATIONS

Symbol	Description	Value
f	Frequency	13.3 MHz
ω	Angular frequency ($= 2\pi f$)	83.57 Mrad/s
λ	Wavelength on the substrate ($= c_{\mathrm{sub}}/f$)	300 µm
ρ_{sub}	Density of the substrate	4.7 g/cm^3
c_{sub}	Surface wave speed on lithium niobate substrate	3,990 m/s
W	Width of microchannel	240 µm
H	Height of microchannel	50 µm
k_0	Wavenumber ($= 2\pi/\lambda$)	20,944 m^{-1}
ρ_{PDMS}	Density of PMDS	1.03 g/cm^3
c_{PDMS}	Bulk speed of sound in PDMS	1,076.5 m/s
ζ	Ratio of displacement amplitude	0.86
C_d	Attenuation coefficient	2,063 m^{-1}
ρ_p	Polystyrene density	1.05 g/cm^3
c_f	Speed of sound in water	1497 m/s
φ_0	Phase shift to achieve zero reference in COMSOL ($= k_0(\lambda - W)$)	1.26 rad

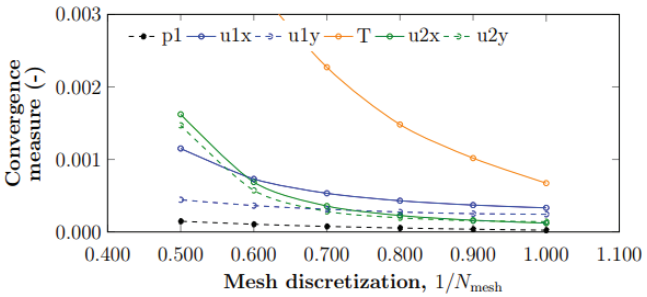

Fig. 2. Mesh convergence analysis vs N_{mesh}. As for $N_{\mathrm{mesh}} = 1.5$ all pressure and velocity terms converge already well below the measure 0.002, and the temperature convergence is only slightly above this limit, we chose $N_{\mathrm{mesh}} = 1.5$ as an adequate trade-off between computational cost and accuracy.

resulting in precise solutions whilst minimizing the required number of degrees of freedom and therefore computational time.

The experimental setup comprised a surface acoustic wave microfluidic device, formed of a PDMS microchannel bonded on top of a lithium niobate 128°Y oriented substrate. The interdigital transducers (IDTs) were designed to resonate at 13.3 MHz, and were driven by a signal generator (TG5012A, Aim-TTi, UK) via LabView (National Instruments, UK). The signal is amplified using power amplifiers (ZHL-1-2W+, Mini-Circuits, UK) to drive the required 24 Vpp voltage to the IDTs. More details on the experimental setup and fabrication are presented in [5].

III. Results

First, a mesh convergence analysis was carried out to reveal the adequate resolution of the mesh in order to capture all thermoviscous-related pressure variations. The method is described by Nama *et al.* [7]: simulations are run for various mesh sizes (controlled by the N_{mesh} value) and compared with an extremely fine mesh solution (where $N_{\mathrm{mesh}} = 0.8$) using the mean-square error as a measure (Fig. 2). This

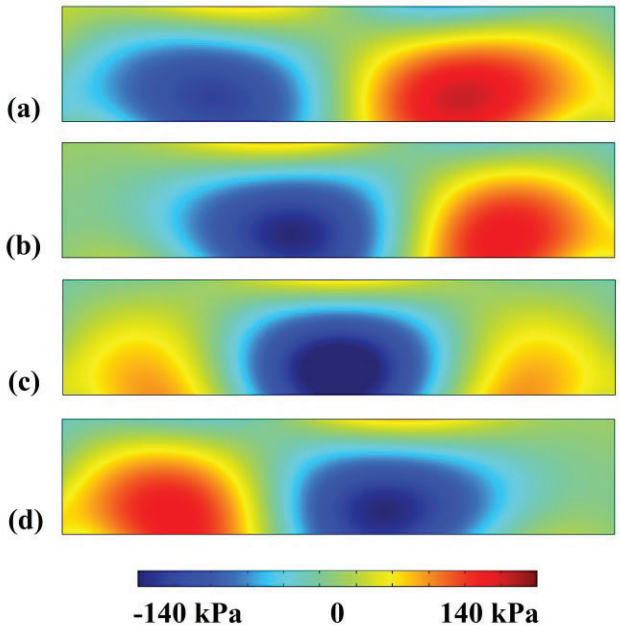

Fig. 3. Pressure distribution within the microchannel for different phase differences between the two transducers: (a) 0° (b) 90° (c) 180° (d) 270°. The colors from blue through green to red correspond to -140 kPa to 140 kPa.

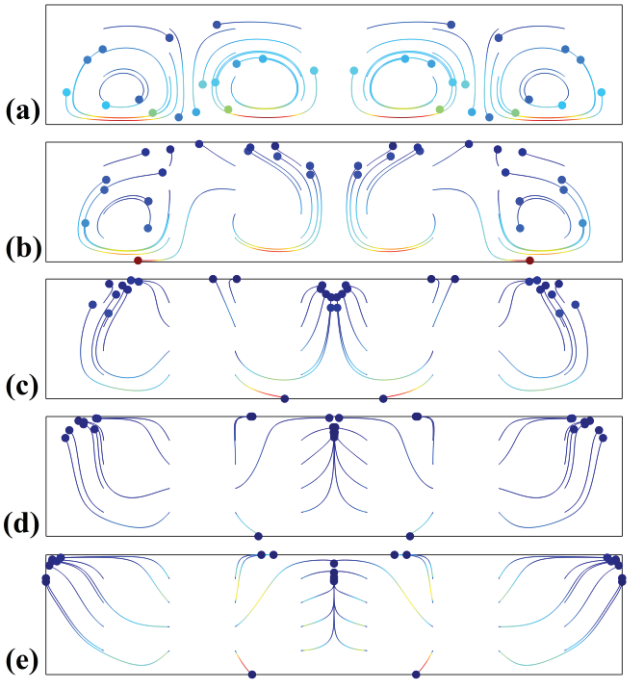

Fig. 4. Analysis of the effect of particle size on trapping efficiency and identification of critical particle diameter. Simulation results of particle trajectories and final particle positions including primary acoustic radiation force and streaming induced drag force after 2 s for zero phase difference between transducers for (a) 1 µm (b) 3 µm (c) 5 µm (d) 7 µm and (e) 10 µm diameter polystyrene particles. For particle sizes below 3 µm, streaming induced effects dominate, while above 7 µm size particles are mainly trapped by the primary radiation force.

analysis revealed that the mesh size $N_{\mathrm{mesh}} = 1.5$ is adequate, resulting in 35,890 domain elements and 2,820 boundary elements and a total number of degrees of freedom of under a million for both the acoustics and flow modules. This resolution was applied for all following investigations.

The relationship between the peak pressure amplitude and the SAW amplitude was studied in order to use an excitation parameter that corresponds to the experiments. Simulations from 0.05 nm to 0.5 nm surface displacement amplitude were

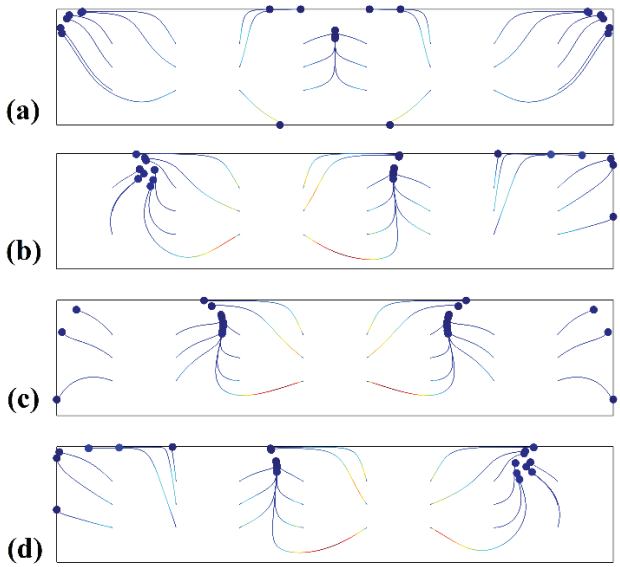

Fig. 5. Illustration of trapping of a 10 µm polystyrene particle within the microchannel for various phase difference values between the two transducers: (a) 0°, (b) 90°, (c) 180° and (d) 270°.

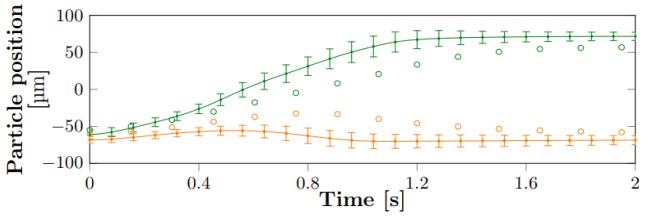

Fig. 6. Experimental (solid lines) and numerical (circles) particle trajectories for separation of 10 μm (orange) and 15 μm (green) polystyrene particles. Error bars are also indicated for both particle sizes.

carried out and the recorded pressure maxima showed a linear relationship as $p_0 = 241.2 d_0$ where the pressure is in kPa and the displacement amplitude in nm.

Pressure distribution within the microchannel at various phase differences can be seen in Fig. 3. For 0° phase, the pressure distribution is symmetric, with a pressure node in the centerline of the channel. As the phase difference between the right and left transducers increases, the pressure pattern moves rightwards as expected. For 180° phase difference, the pressure distribution is again symmetric with a pressure antinode at the centerline of the channel.

The streaming velocity field was generated using the solutions from the thermoviscous acoustics module for the pressure and velocity fields. We identified the critical particle size in our device by running simulations for particles with diameter ranging from 1 μm to 15 μm, originally dispersed in a 3 by 8 grid within the microchannel. The final particle locations after 2 s and trajectories can be seen in Fig. 4. For particle sizes of range 1-3 μm, movement is dominated by streaming, as the particles are not trapped at well-defined spatial positions but follow the vortices of the streaming velocity field. Above 7 μm, the particles behave in the usual manner by trapping at the nodes of the pressure field. Between 3-7 μm particle size, streaming and radiation force effects are of similar magnitude and particles neither follow streaming vortices nor are trapped at the pressure nodes.

To further investigate the effect of phase difference between the transducers on the trapping of the particles, a similar investigation, as presented in Fig. 4, was carried out, with fixed particle size (10 μm polystyrene) and by changing phase difference. The results of this analysis can be seen in Fig. 5: for zero phase difference, the particles are trapped at the middle of the channel. As the phase is gradually increased, this trapping location moves to the right. For 180° phase difference, where the pressure antinode is aligned with the centerline of the channel, the particles are pushed away from this position towards the two pressure nodes located symmetrically on the two sides (Fig. 5c). A comparison with Fig. 3 further validates this effect: the zero pressure nodes in Fig. 3 coincide well with the trapping positions of the particles in Fig. 5.

As a final verification, the model was compared with experimental separation results for 10 and 15 μm polystyrene particles. The results in Fig. 6 show good agreement between the experiments and the trajectories. The only fitting parameter for the trajectories was the pressure amplitude, applied via the surface displacement of the surface acoustic wave as discussed earlier in the paper.

ACKNOWLEDGMENT

G. S. would like to thank Heriot-Watt University for their financial support for the conference.

IV. CONCLUSIONS

In this paper we presented a numerical investigation of a surface acoustic wave device, utilizing a thermoviscous acoustics module coupled with a laminar flow module to capture both the primary radiation force and streaming drag forces accurately. The model was first applied to investigate the critical particle diameter in a channel that is not integer multiple width of half the wavelength and identified that this particle size was between 3 and 7 μm. Below this value, particles follow the streaming rolls and move in vortices without trapping. Above this particle size, the particles trap at the pressure nodes within the channel. Validation of this trapping for various phase differences between the two transducers was also shown for 10 μm particles. Direct extension of the model by a discretized phase-stepping allowed for simulating separation trajectories for 10 and 15 μm polystyrene particles, which were in excellent agreement with experimental results.

REFERENCES

[1] C. W. Shields, C. D. Reyes, and G. P. Lopez, "Microfluidic cell sorting: a review of the advances in the separation of cells from debulking to rare cell isolation," *Lab Chip,* vol. 15, no. 5, pp. 1230-49, Mar 7 2015.

[2] D. R. Gossett *et al.*, "Label-free cell separation and sorting in microfluidic systems," *Analytical and Bioanalytical Chemistry,* vol. 397, no. 8, pp. 3249-67, Aug 2010.

[3] M. Wiklund, "Acoustofluidics 12: Biocompatibility and cell viability in microfluidic acoustic resonators," *Lab Chip,* vol. 12, no. 11, pp. 2018-28, May 8 2012.

[4] G. D. Skotis, D. R. Cumming, J. N. Roberts, M. O. Riehle, and A. L. Bernassau, "Dynamic acoustic field activated cell separation (DAFACS)," *Lab Chip,* vol. 15, no. 3, pp. 802-10, Feb 7 2015.

[5] G. Simon *et al.*, "Particle separation by phase modulated surface acoustic waves," *Biomicrofluidics,* vol. 11, no. 5, p. 054115, Sep 2017.

[6] G. Simon *et al.*, "Particle separation in surface acoustic wave microfluidic devices using reprogrammable, pseudo-standing waves," *Applied Physics Letters,* vol. 113, no. 4, 2018.

[7] N. Nama, R. Barnkob, Z. Mao, C. J. Kahler, F. Costanzo, and T. J. Huang, "Numerical study of acoustophoretic motion of particles in a PDMS microchannel driven by surface acoustic waves," *Lab Chip,* vol. 15, no. 12, pp. 2700-9, Jun 21 2015.

[8] C. Devendran, T. Albrecht, J. Brenker, T. Alan, and A. Neild, "The importance of travelling wave components in standing surface acoustic wave (SSAW) systems," *Lab Chip,* vol. 16, no. 19, pp. 3756-3766, Sep 21 2016.

[9] H. Bruus, "Acoustofluidics 7: The acoustic radiation force on small particles," *Lab Chip,* vol. 12, no. 6, pp. 1014-21, Mar 21 2012.